A Fission Heated Subassembly for Sodium Boiling Experiments in EBR-II

by

LAURIN RALPH DODD

A thesis submitted in partial fulfillment

of the requirements for the degree of

Master of Science in Nuclear Engineering

University of Washington

1976

Approved by_____
(Chairperson of Supervisory Committee)

Program Authorized
to Offer Degree_____

Date_____

DISCLAIMER

In presenting this thesis in partial fulfillment of the requirements for a Master's degree at the University of Washington, I agree that the Library shall make its copies freely available for inspection. I further agree that extensive copying of this thesis is allowable only for scholarly purposes. It is understood, however, that any copying or publication of this thesis for commercial purposes, or for financial gain, shall not be allowed without my written permission.

Signature_____

Date_____

TABLE OF CONTENTS

LIST OF TABLES

LIST OF FIGURES

LIST OF FIGURES

ACKNOWLEDGEMENTS

The author wishes to express his gratitude to the following individuals and organization for their assistance in the completion of this thesis.

To Dr. Robert W. Albrecht, the author's thesis advisor, for suggesting the topic and providing guidance throughout the endeavor.

To Donald Rowe for making COBRA III-C available.

To Ralph Crow and Steve Artus for their assistance in adapting COBRA III-C to the University computer.

And, finally, to the Reactor Research and Development Division of the Energy Research and Development Administration who made this project possible by providing the necessary funding.

INTRODUCTION

Localized coolant boiling in a liquid metal fast breeder reactor (LMFBR) may be the first indication of a partial coolant blockage in a subassembly. The potential for such an incident to develop into an accident disrupting the reactor core attracts the development of an instrumentation system capable of detecting local coolant boiling. A requisite for the development of such a system is a thorough understanding of the characteristics of the boiling and the signals (neutronic and accoustic) generated. This knowledge may best be obtained by conducting prototypical in-reactor experiments in which local coolant boiling is generated downstream of a simulated blockage.

A conceptual design of a 37 pin, fission-heated subassembly containing a central blockage is presented here. The subassembly is designed to operate in Experimental Breeder Reactor II (EBR-II), a liquid sodium cooled, fast reactor, the only one presently operational in the United States.

A boiling experiment to be performed with a fission-heated subassembly in EBR-II may be regarded as but one in a series of boiling experiments which may be necessary to determine both the ultimate need for and, then, the design information required for an instrumentation system capable of detecting local boiling in a commercial LMFBR. Ideally, experiments with a gamma-heated subassembly[1] would precede fission-heated experiments. Such experiments could provide valuable information on the response of the reactor and instrumentation to coolant boiling in a safe, relatively inexpensive subassembly. Then, the performance of an experiment utilizing a fission-heated subassembly containing a blockage would provide information relevant to the localized, subcooled boiling

which is more characteristic to the reactor incident being considered, and is almost certainly a prerequisite for any boiling experiments that may be performed in a future reactor more prototypical of a commercial LMFBR.

It is of interest to briefly consider the mechanism involved in the initiation and propagation of an incident arising from a coolant channel blockage in an LMFBR. In large-scale LMFBRs, the fuel pins are typically grouped in bundles (subassemblies) of 200 - 300 pins and each group is contained in a hexagonal, stainless steel can. The pins typically have a diameter of just less than a quarter of an inch and are very closely spaced with clearances between pins of about .05 inches. Pin spacing is maintained by either wrapping the elements with a small diameter wire or by using grid-type spacers at axial intervals of six to eight inches. Wire wraps have thus far enjoyed more popularity in the US while grid spacers are generally being utilized in Europe.

It is the close pin spacing, unique to the LMFBR, that is primarily responsible for the concern relating to coolant channel blockages. With close pin spacing and with locally reduced flow areas due to pin spacing devices (particularly grid spacers[2]) or pin distortion, it has been postulated that debris carried by the coolant may accumulated in one of these already rather restricted flow areas causing a blockage.[2-7] Sources of debris in the coolant include corrosion products and particles from failed fuel elements. Conventional LMFBRs have filters to remove coolant debris, but smaller particles may pass through the filters and there is no protection against debris generated within the subassembly.

The predicted chain of events following the occurrence of a blockage is outlined in figure 1.[2,6,7] Decreased heat removal in the vicinity of the blockage causes overheating, possible clad failure, and, if fuel

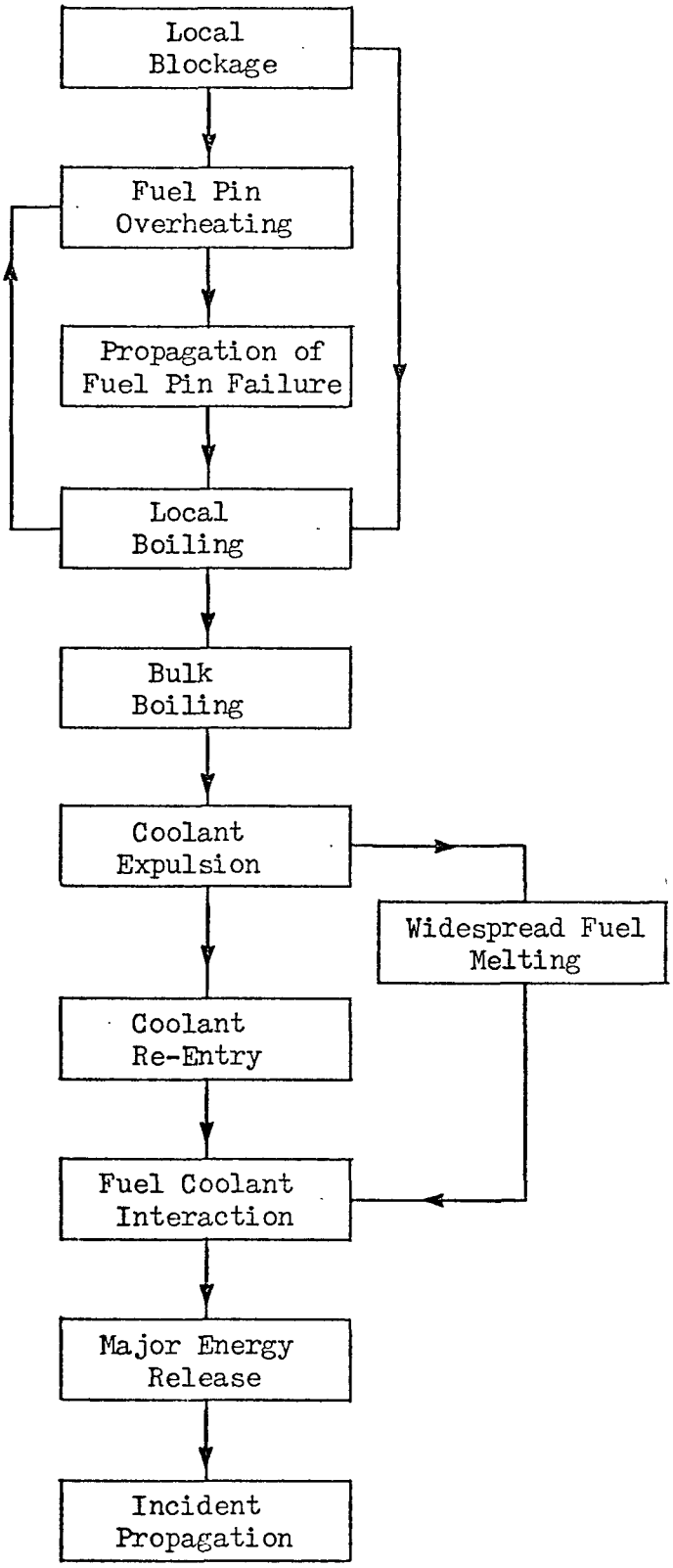

Figure 1. Chain of Events Leading from Local Blockage to Major Incident (from reference 2)

melting occurs before clad failure, a release of molten fuel may also occur. Both the pressure of the released fission gas and the molten fuel - coolant interaction have the potential to damage neighboring elements. The blockage may grow due to a further accumulation of debris causing a further decrease in heat removal capabilities. When the blockage becomes large enough, local boiling of the coolant will occur immediately downstream of the blockage. Further propagation of the blockage will eventually lead to bulk boiling which can cause a significant portion of the coolant to be expelled from the subassembly, causing widespread fuel melting. Upon re-entry of the coolant, the theoretically predicted energy released due to the molten fuel - coolant interaction is large enough to propagate the incident to neighboring subassemblies.

An important question in the process outlined above is whether or not local boiling will precede significant fuel failure. If it does not, it is possible that existing failed fuel detectors may detect the incident,[8] thus negating the need for further instrumentation. The size of blockage required to cause local boiling is a function of the size of the subassembly, the location and permeability of the blockage, and whether or not the blockage is comprised of fissionable material. It has been estimated that a blockage of about 12% of the available flow area (about 100 coolant channels) of a PFR subassembly (325 pins per bundle) is necessary to cause local boiling,[2] while about a 40% - 50% flow area restriction is necessary for boiling in a SNR-300 subassembly[2,8] (169 pins per bundle). The size of blockage necessary to cause significant fuel element failure is not known.

DESIGN DESCRIPTION

The primary considerations in the subassembly design were that geometry, materials, and operating conditions in the region where boiling is to occur be as representative as possible of a commercial LMFBR subassembly, and that the subassembly would perform safely in an instrumented subassembly position (INSAT) of EBR II for a period of time sufficiently long to allow boiling experiments to be conducted. Deterioration of material properties and excessive pressure from fission gas buildup likely precludes leaving the subassembly in the reactor for the full length of the normal EBR-II operating period.

The subassembly (figure 2) is comprised of seven regions. Coolant enters the lower adaptor from the high pressure coolant plenum of the reactor. It is orificed past the lower particle collector and then routed into the lower flowmeter. From the flowmeter, the coolant flows through an orifice plate into the fuel element region, through the upper particle collector screen, through the upper flowmeter, and then through the upper adaptor where it is released to the outlet plenum of the reactor.

The lower adaptor seats in the upper grid plate of EBR II and is orificed to provide the necessary coolant pressure loss so that the proper flow rate is obtained.

The lower and upper particle collectors reduce the likelihood of gross flow restrictions outside of the fuel element region and prevent particles of significant size from leaving the subassembly in the event of a mechanical failure.

The flow meters monitor flow fluctuations and may be used for boiling detection.

The fuel element region is comprised of 37 pins arranged in a tri-

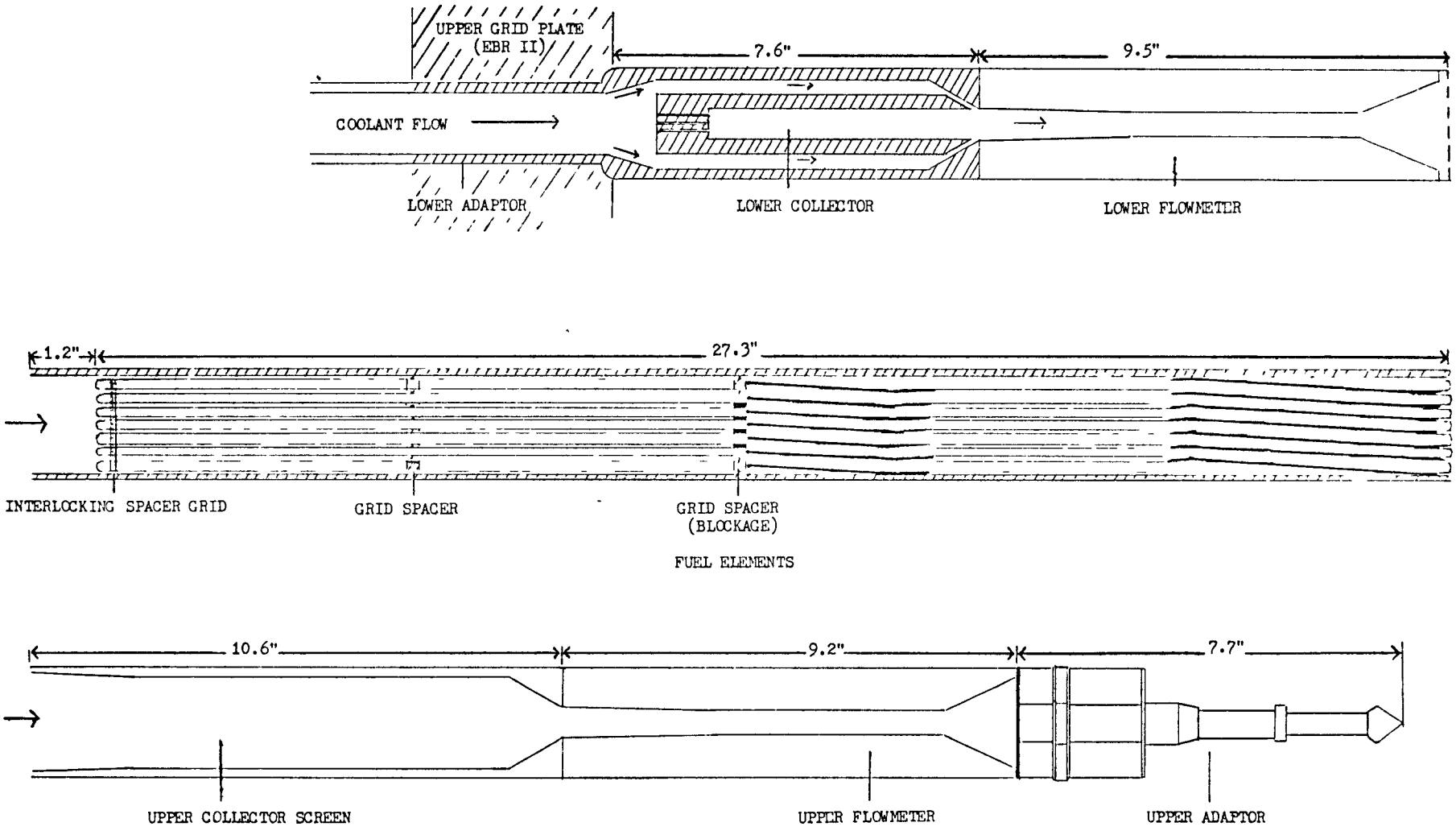

Figure 2. Lateral View of the Subassembly

angular pitch in four rows (figure 3). A honeycomb grid containing a centrally-located 24 channel blockage (figure 4) is located at the core midplane elevation. The pins are supported axially by an interlocking spacer grid. Proper pin spacing is maintained by a honeycomb grid located midway between the interlocking grid and the grid containing the blockage and by wire wrap spacers above the blockage.

The outer row of elements (18 pins) are stainless steel "dummy" pins (figure 5). They serve as structural support for the spacers grids, conduits for the leads to the lower flowmeter, and provide an effective barrier for the propagation of coolant boiling in the radial direction. The latter function is provided by maintaining the coolant temperature in the region between the subassembly wall and the boiling region at about 1000° F subcooled.

The fuel elements in the inner rows (19 pins) are comprised of three regions (figure 5). In a region starting at the blockage and extending four inches downstream of the blockage, the fuel is highly enriched (65%) UO_2. The remainder of the core region is slightly enriched (3%) UO_2 and the remaining length of the pins is to be constructed of either stainless steel or filled with depleted UO_2 plugs. This arrangement provides a relatively high heat flux in the region where boiling is desired while maintaining subassembly outlet temperatures within permissable limits. The stainless steel (or depleted UO_2) plugs aide in meeting the EBR II shielding requirements without sacrificing characteristic flow paths.

The wire wrap spacers may be spot welded or brazed to the clad at several axial locations. The wrap diameter is .040 inches while the pin spacing at room temperature is .045 inches. This allows for thermal expansion of the pins at temperatures up to about 1800° F without adding

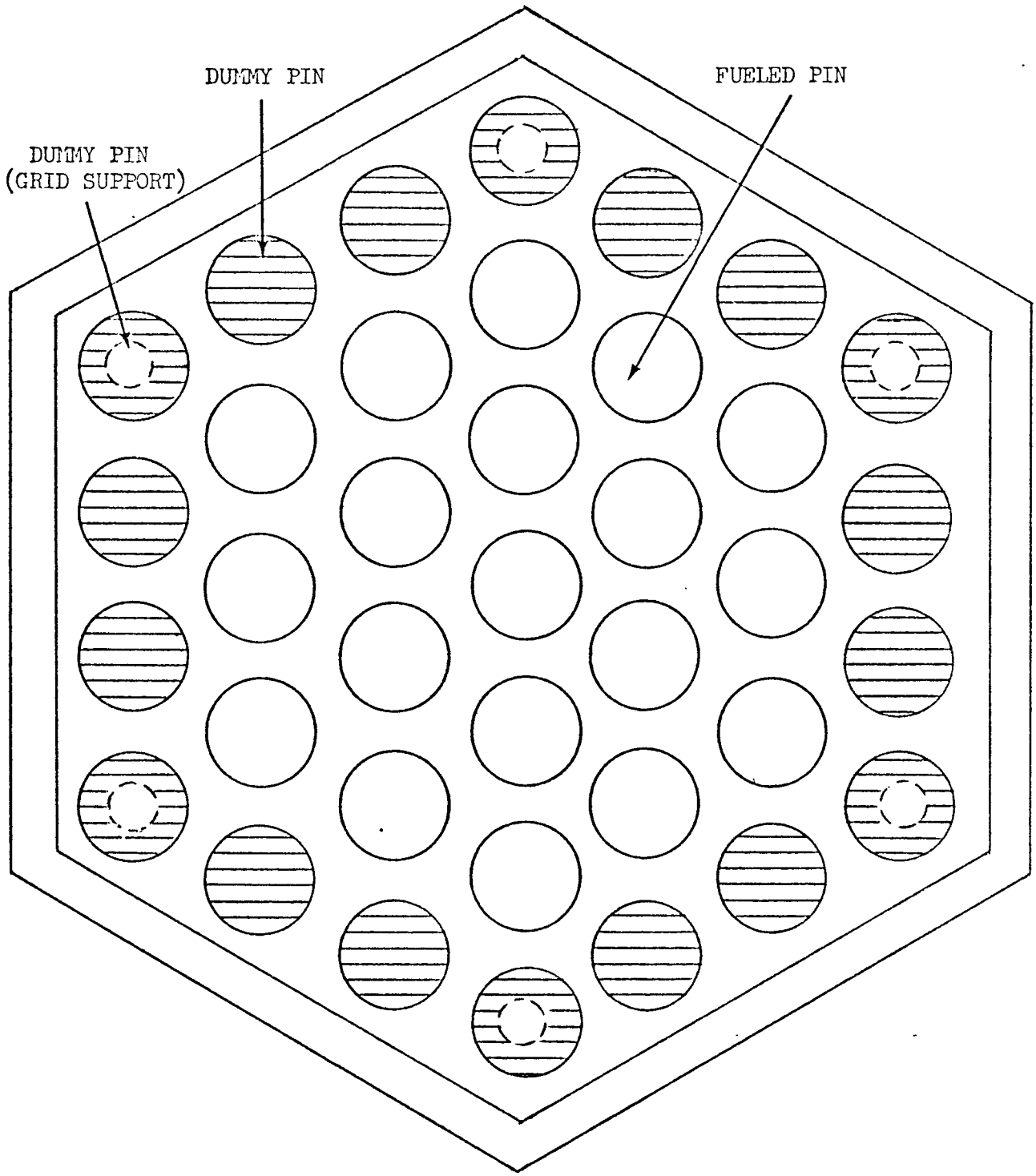

Figure 3. Arrangement of Fuel and Dummy Elements

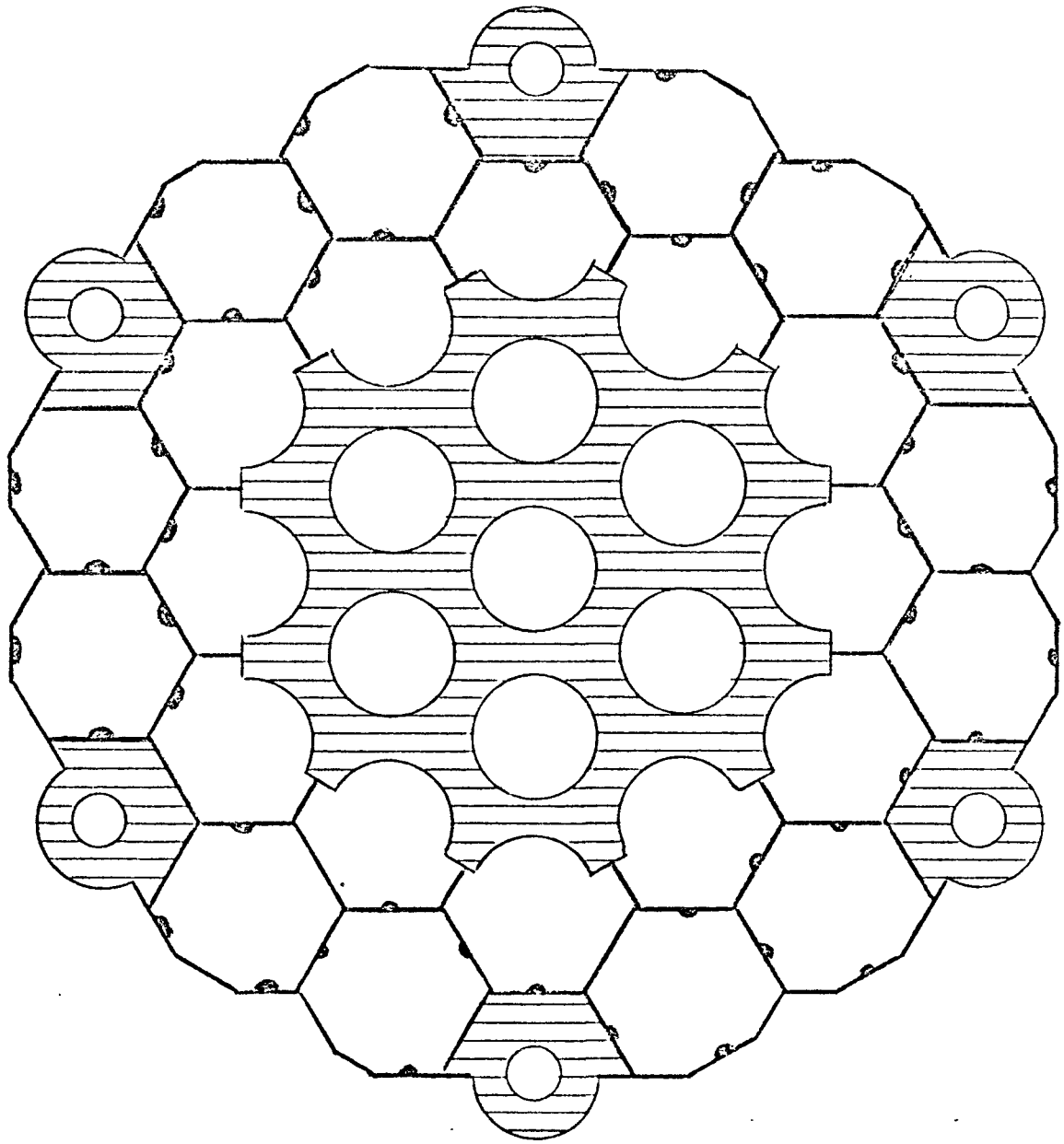

Figure 4. Honeycomb Grid with Blockage

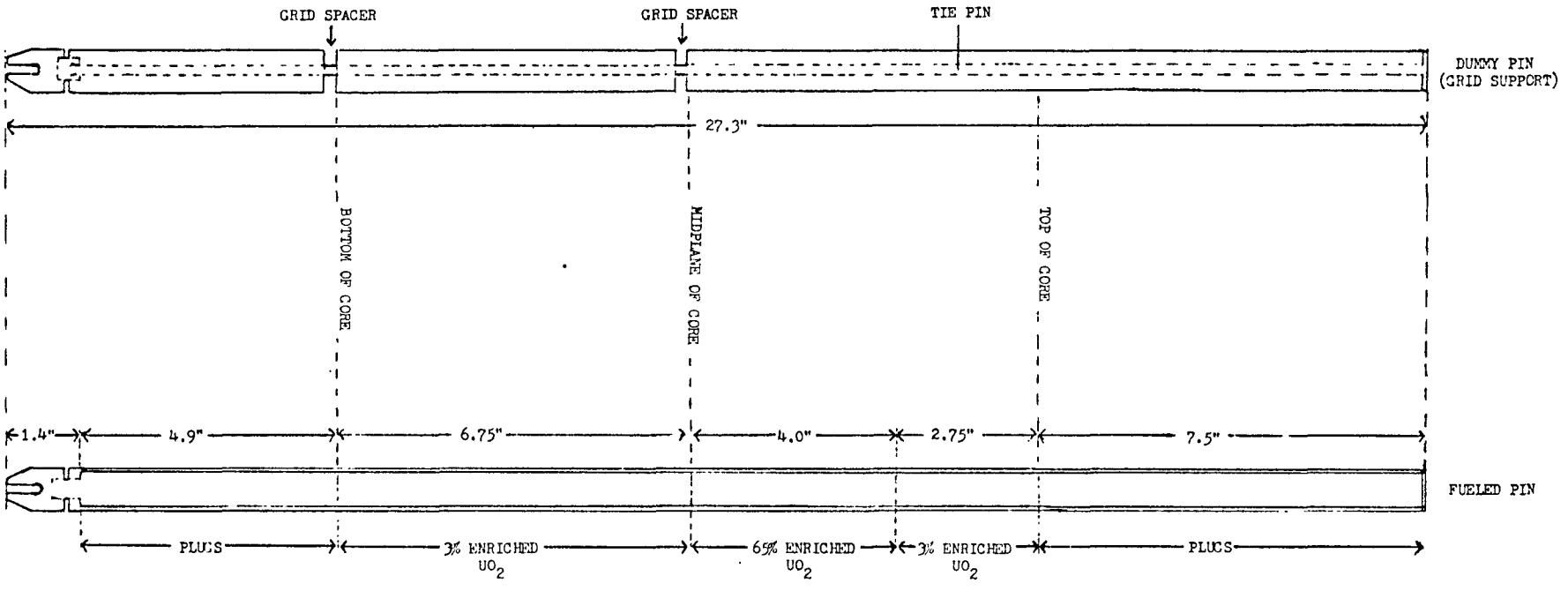

Figure 5. Fuel and Dummy Elements

large stresses from contacts between the pins and wraps. Some spacers will contain thermocouples for monitoring coolant temperatures.

Table 1 lists the relevant design parameters of the subassembly and compares them with those of a Fast Test Reactor (FTR) subassembly which may be considered to be representative of a commercial LMFBR. The design criteria for an instrumented subassembly in EBR II is listed in Table 2.

It is noted from Table 1 that there are three design parameters that are rather unsimilar to FTR. Namely, the cross-section of the subassembly can is considerably smaller than that of FTR, the maximum linear power is about two-thirds that of FTR, and the coolant flow rate is considerably less in the design. The smaller subassembly can is primarily responsible for the reduced flow rate which is required to assure that boiling occurs, but, other than this effect, the smaller geometry has no influence on the characteristics of the boiling region. The decrease in the maximum linear power is a result of a small fuel diameter in the design and a lower flux level in EBR II as compared to FTR. The decreased fuel diameter is a result of using a thick clad while maintaining a prototypical pin diameter and is also due to the relatively large fuel-clad gap which prevents the fuel from exerting large pressures on the clad due to thermal expansion. This arrangement also makes the possibility of fuel melting extremely unlikely.

TABLE 1

COMPARISON OF DESIGN PARAMETERS WITH FTR

Parameter	Design	FTR
flat-flat distance (in)	1.907	4.3
pins per subassembly	37	217
pin diameter (in)	.230	.230
pin pitch (in)	.275	.285
pin length (in)	27.3	92.0
maximum linear power (watts/cm)	298	450
clad thickness (in)	.020	.015
hydraulic diameter (in) (not including peripheral channels)	.133	.159
subchannel flow area (sq in)	.012	.0144
subassembly flow rate (gal/min)	9.66	55.0
coolant mass flux (lb/(hr sq ft))	0.5×10^6	3.8×10^6
subassembly wall thickness (in)	.08	.12
fuel type	U-oxide	mixed oxide
theoretical density (%)	93	90.4
smear density (%)	90.2	85.3
diametrical fuel-clad gap (in)	.006	.0055
fuel-clad bonding	helium backfill (1 atm)	
bundle average outlet temperature ($^\circ$ F) (full reactor power)	950.5	
Blockage Parameters:		
number channels blocked	24	
effective blockage radius, L_B (in)	.500	
blockage thickness, w (in)	.250	
flow area blocked, A_B (sq in)	.288	
nominal flow area, A_0 (sq in)	1.106	

TABLE 2

REFERENCE DESIGN CRITERA FOR INSTRUMENTED SUBASSEMBLY (INSAT)[9]

number INSAT positions	2
core locations	converted control rod positions in 5th row of EBR II
configuration	hex tube
material	304 stainless steel
dimensions (in)	
across flats	1.902/1.912
inside flats	1.824/1.830
overall length (less lead length)	93.6
coolant temperature at inlet (^{o} F)	700
allowable coolant outlet temperature (^{o} F)	848 - 1048

DESIGN ANALYSIS

Power Distributions

The relative axial power distributions for fuel and dummy elements are shown in figure 6. The profiles were calculated using gamma and fission heating rates from the EBR II experimenter's guide.[9] Detailed procedures may be found in Appendix A.

The total subassembly power at full reactor power (62.5 Mwt) is calculated to be 87.0 Kwt and is distributed among the various elements as shown in Table 3.

TABLE 3

COMPONENT POWER DISTRIBUTION
(Full Reactor Power)

Component	Power (Kwt)	Number	Total (Kwt)	Fraction of Total
fuel element	3.98	19	75.6	.869
dummy element	.473	18	8.51	.098
subassembly wall	.478	6	2.87	.033

It should be noted that although the axial power profile is rather untypical of a commercial LMFBR, it has the advantage of supplying a relatively high heat flux in the region where boiling is desired without raising subassembly outlet temperatures beyond the allowable limit established for an INSAT position of EBR II (Table 2). The profile within the boiling region itself is typical of the mid-core region of a typical LMFBR.

The peak heat flux in the subassembly at full power is $.514 \times 10^6$

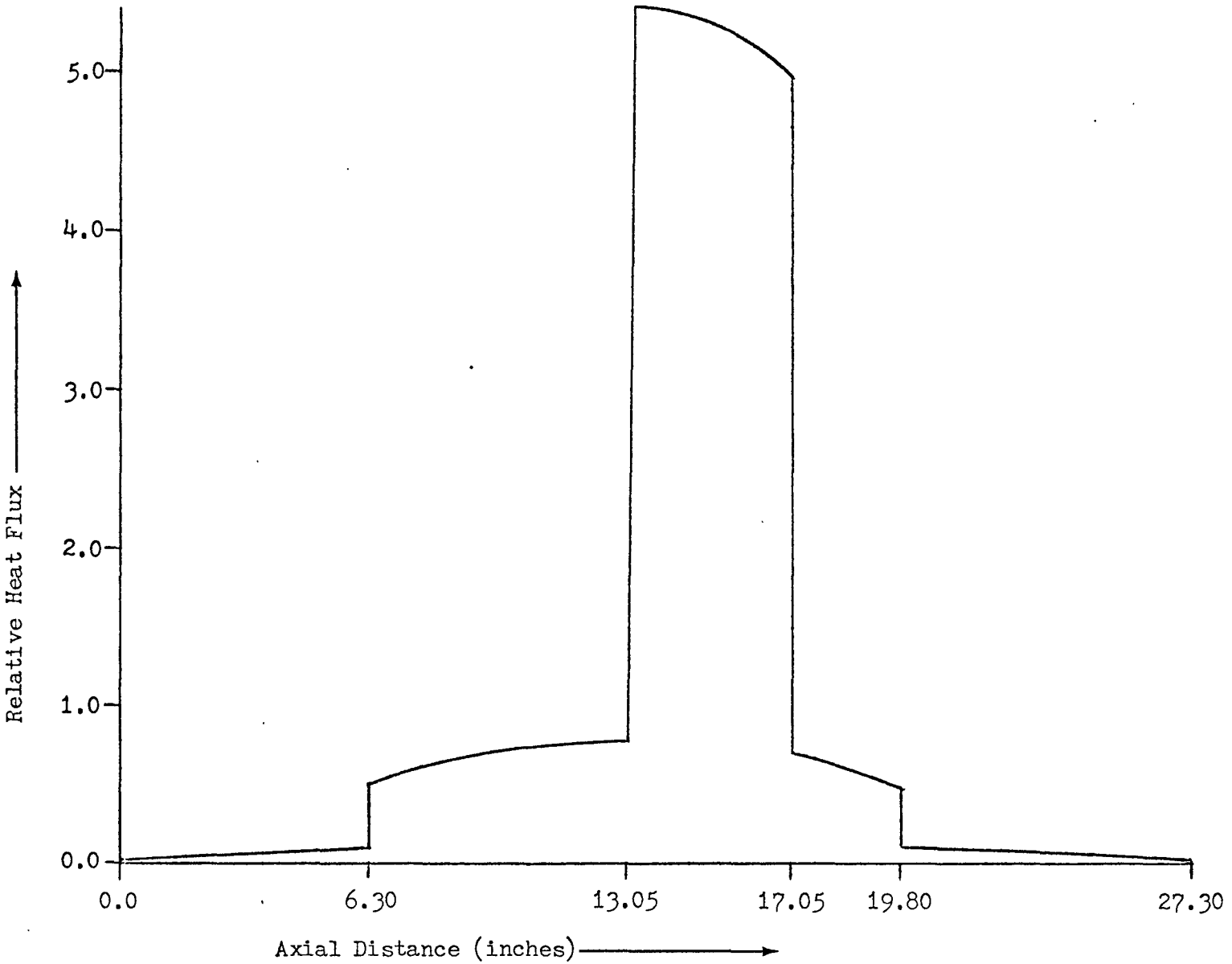

Figure 6. Relative Axial Heat Flux

Btu/(hr ft^2) and occurs immediately downstream of the blockage. This is considerably less than the design value of .8 x 10^6 Btu/(hr ft^2) for FTR.

Coolant Temperatures - Upstream of Blockage

Coolant temperatures upstream of the blockage are influenced little by the presence of the blockage, and then the influence is only within a very short distance of the blockage (about one inch). Thus temperatures may be calculated with any standard subchannel thermal-hydraulic code. COBRA III-C was utilized for this design. A description of this code may be found in reference 10; input data used is located in Appendix B.

Coolant Temperatures - Behind Blockage

It has been demonstrated that the nature of the flow downstream of a disc located perpendicular to the coolant flow in a rod bundle is very similar to that of the case of a simpler geometry without rods.(3) A distinct region of recirculating flow with standing eddies develops downstream of the blockage, but there is no flow detachment upstream. The wake (region of recirculating flow) is bounded by a zero streamline extending from the edge of the blockage to a point L_R downstream of the blockage (Figure 7). There is no net mass transfer across the zero streamline, but turbulent mass exchange does occur.

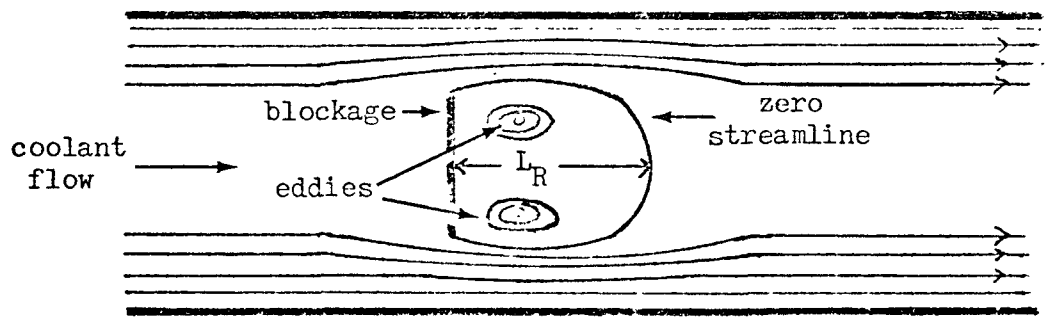

Figure 7. Qualitative Description of Coolant Flow Downstream of Blockage

Temperature distributions for the wake region are very difficult to predict theoretically.[11] Typical thermal-hydraulic codes such as COBRA III-C are unable to describe regions of reverse flow because the governing conservation equations have lost their elliptic form due to the simplifying assumption of a preferred flow direction. (Apparently, COBRA IV, when published, will have overcome this limitation.[12])

Gregory and Lord, of the Dounreay Experimental Reactor Establishment in Great Britain, have proposed a method for estimating the maximum and mean temperatures in the wake by using a simple heat balance and a parameter calculated by a code they developed that solves the conservation equations in their elliptic form for a simplified geometry.[2] The method used is both simple and the only one known to be available for making these estimates. Consequently, the method, with some modification, is utilized for estimating wake temperatures in this design. A description follows.

If it is assumed that the only thermal mixing that occurs between the wake region and the bypass flow is due to turbulent mass exchange, then the mean coolant temperature difference between the wake and the bypass flow is given by:

$$T = \frac{q_c t}{p\, c_p} \qquad \text{Eq. 1}$$

where:

q_c = coolant specific power within the wake (total power generated within wake divided by volume of coolant in wake)

t = mean time of residence in the wake by a fluid particle

p = coolant density

c_p = heat capacity of the coolant

The mean residence time, t, is a value that has been determined experimentally for various subassemblies by measuring the mass of liquid within the wake, M_w, and the rate of turbulent mass exchange between the wake and bypass flow, m. In this case, t is given by:

$$t = \frac{M_w}{m} \qquad \text{Eq. 2}$$

Gregory and Lord, using the code WAKE, calculate this parameter directly. A brief description of their assumptions and results follows.

The code WAKE simulates a fuel subassembly by considering a cylinder with a hydraulic diameter equivalent to that of the subassembly with fuel. The effect of the fuel pins on the flow is represented by an anisotropic viscosity. The heat source is represented by a uniformly distributed source in the coolant having the same power to flow ratio as the subassembly. Mixing is assumed to be due to turbulence only. The conservation equations are coupled to a turbulence model containing an empirical constant and are solved to yield velocity and temperature profiles within the wake. The residence time is calculated from a converged flow solution rather than by equation 2.

Calculations with WAKE have resulted in the following relationship for determining the residence time (the denominator has been determined from a graphical representation in reference 2):

$$t = \frac{L_B \left(1 - \frac{A_B}{A_O}\right)}{a + bRe} \qquad \text{Eq. 3}$$

where:

L_B = blockage radius

A_B = flow area which is blocked

A_O = nominal flow area

Re = Reynolds number far from blockage

$a = -.285$

$b = 1.354 \times 10^{-4}$

The form of equation 3 is somewhat predictable considering equation 2, as it would be expected that the mass of the liquid in the wake would be proportional to the cube of some characteristic length, L_C, and that the turbulent mass exchange rate would be proportional to the surface area of the wake, L_C^2, and to the inlet mass velocity. Gregory and Lord determined that the blockage radius, L_B, was an acceptable characteristic length in determining this relationship. The factor $(1 - A_B/A_O)$ accounts for the increased turbulence due to an increase in the velocity of the bypass flow at the plane of the blockage.

Comparisons of residence times calculated with WAKE were made with those obtained from experiments using mockups of two different subassemblies, one being a four-times full-scale mockup representing a 60° sector of the first six rows of a PFR subassembly and the other was a full-scale mockup of a SNR subassembly. Both utilized water as the coolant. The PFR experimenters considered blockages of 13%, 30% and 40% of the available flow area, while blockages of 15% and 41% were used in the SNR mockup. Gregory and Lord found that modified values of theoretical and experimental residence times $(t/(1 - A_B/A_O))$ agreed fairly well over the range of Reynolds number investigated $(2 \times 10^4 - 1 \times 10^5)$, though the trend was for the theoretical value to be higher than the experimental value, particularly at the higher Reynolds numbers, where the difference was about 20%.

Two important points should be made. First, it is to be expected that experimentally measured residence times are too long because they

are generally measured by determining the decrease as a function of time of a tracer in the wake after an abrupt interruption of its injection from a point source in the center of the wake.[3] Injection from the point source rather than a distributed source leads to underestimates of the turbulent mass exchange rate and, therefore, overestimates of the residence time (eq. 2). This tends to widen the difference between residence times calculated by WAKE and experimental values. The second point is that temperature increases predicted by equation 1, using residence times given by equation 3, are consistently twice the values as those calculated directly by WAKE. Gregory and Lord offer several possible qualitative explanations why their calculated residence times may be large. For design purposes it is assumed that the value of the residence time is somewhere between the value given by equation 3 and the value necessary to give temperature increases as predicted by WAKE, i.e. one-half the value given by equation 3. Thus, for design estimates, equation 3 is replaced by:

$$t = (0.75 \pm 0.25) \frac{L_B \left(1 - \frac{A_B}{A_0}\right)}{a + bRe} \qquad \text{Eq. 4}$$

Thus far it has been assumed that mixing occurs only through turbulence. Kirsch has shown that this is approximately true for Re_{BL} greater than about 10^6, where Re_{BL} is the Reynolds number obtained using the blockage diameter as the characteristic length.[3] He estimates, conservatively, that molecular heat transport in this case is less than 5% of the turbulent heat transport. The value of Re_{BL} in this design is about 3×10^4, so thermal conduction between the wake and bypass flow may not be neglected. This effect is taken into account by using a rather

simple conduction model (Appendix A), resulting in equation 1 being replaced by:

$$T = \frac{.1054\ q''}{11.4 + \frac{14.5}{t}} \times (\text{fraction operating power}) \qquad \text{Eq. } 5$$

where q'' is the average heat flux in the wake (Btu/(hr ft^2)).

Equation 5 yields an estimate of the mean temperature in the wake. WAKE results indicate that the ratio of maximum to mean wake temperatures is less than 2 and, generally, about 1.6. Table 4 lists the mean and maximum wake temperatures for various flow rates as calculated using equation 5, assuming operation at full reactor power and an average temperature of the bypass flow of 800° F.

TABLE 4

MEAN AND MAXIMUM WAKE TEMPERATURE RANGES FOR VARIOUS FLOW RATES

Flow Rate (10^6 $\frac{lb}{hr\ ft^2}$)	Re (at S/A inlet)	t (sec)	T mean (°F)	T max (° F)
3.0	4.7×10^4	$.045 \pm .015$	909 - 1012	974 - 1140
2.0	3.2×10^4	$.069 \pm .023$	965 - 1118	1063 - 1309
1.0	1.6×10^4	$.15 \pm .05$	1144 - 1441	1350 - 1825
0.6	$.9 \times 10^4$	$.27 \pm .09$	1385 - 1840	1735 - 2464
0.5	$.8 \times 10^4$	$.34 \pm .11$	1522 - 2032	1955 - 2773
0.4	$.6 \times 10^4$	$.47 \pm .16$	1724 - 2362	2278 - 3299

The effects of the wire wraps on wake temperatures have, thus far, been neglected. Qualitatively, it would be expected that wire wraps could effectively increase the maximum to mean temperature ratio in the wake as the wraps could effectively trap the coolant between the blockage and wrap

at some locations. Experiments conducted at ORNL with a mockup of a FTR subassembly indicate that such trapping may occur, but that the temperature variations are not great compared to the overall temperature rise behind the blockage.[13]

The results in Table 4 predict that boiling will occur for the design flow rate of 0.5×10^6 lb/(hr ft^2), even if the residence time is the shortest value predicted. Boiling may occur for flow rates up to twice this value, but the uncertainty in the residence time discourages the use of higher flow rates.

The location of the maximum temperature in the wake would be immediately downstream of the blockage, at the edge of the wake, were it not for thermal conduction through the blockage. This is because coolant is continually heated as it enters the recirculating flow at the edge of the wake traveling in an upward direction, flows back down through the center of the wake, and is heated further as it travels radially outward. Experiments have shown that radial temperature profiles immediately downstream of a blockage are relatively flat, and, in some cases, are double-humped because of the motion described above; but the maximum temperatures in the axial direction are located some distance downstream of the blockage due to conduction through the blockage.[2,3] The ORNL experiment showed maximum temperatures about one inch downstream of a stainless steel blockage of .2 in thickness. For design purposes, it is assumed that the maximum temperature occurs .75 in downstream of the blockage and that the radial temperature profiles within the wake are flat.

Using a mean temperature of 800° F for the bypass flow at full power and a saturation temperature of 1800° F, it is predicted (Appendix A)

that boiling will occur at somewhere between 52% and 89% of full power for the design flow rate.

Coolant Temperatures - Downstream of Blockage

Though some existing thermal-hydraulic codes may be moderately successful in predicting temperature distributions downstream of an impermeable blockage,[13] it was found that the flow solution in COBRA III-C would not converge for this case because of the large diversion cross-flows in the vicinity of the blockage. It is useful to make rough estimates of the axial temperature profile in this region for use in estimating thermal stresses.

Computations were performed using COBRA III-C for a subassembly (one-sixth geometry - figure 8) containing no blockage and for one containing a permeable blockage which allowed 18% residual flow through the blockage. For the latter case radial temperature profiles downstream of the wake had rather extreme peaks on the subassembly axis. It is believed that such extreme peaking would not occur for the case of an impermeable blockage because the coolant entering this region would have undergone a more thorough thermal mixing in moving through the unheated region outside the periphery of the wake. For design purposes, axial temperature distributions downstream of the wake are assumed to be those found by averaging the temperatures at each axial point in channels directly behind the blockage (channels 1 - 4) and in channels of unrestricted flow (channels 5 - 12), both calculations being performed for the case of the permeable blockage. The profiles for full power are shown in figure 9.

Temperature profiles in figure 9 were calculated neglecting wire wraps, as a rigorous calculation with wire wraps requires a full 37 pin

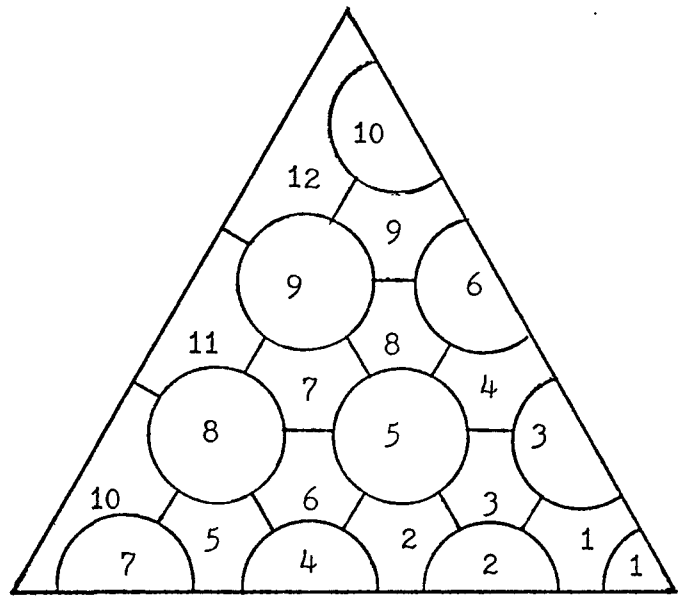

Figure 8. One-sixth Geometry Model Used in COBRA III-C (Blockage in channels 1, 2, 3, and 4)

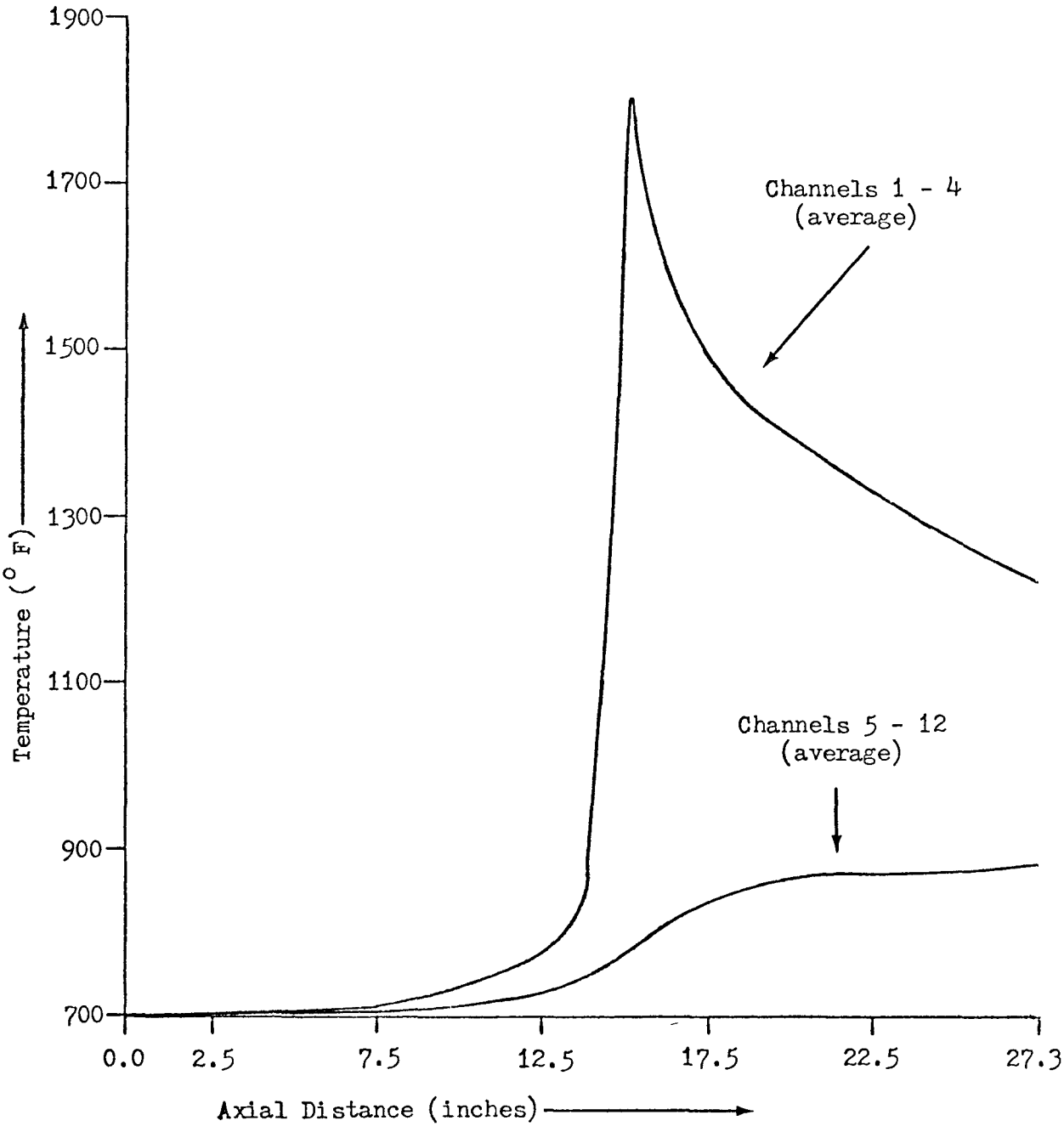

Figure 9. Axial Temperature Profiles (full reactor power)

model which requires a computer of larger capacity than the one available. An estimate of the effect of wire wraps was made by using a one-sixth geometry model including wire wraps and considering only inner channels (channels 3 and 7). The primary effect was to increase mixing between channels to such an extent so as to reduce the mean difference between channel and bundle-average outlet temperatures by about 35%, as compared to the unblocked case without wraps.

It should be kept in mind that profiles in figure 9 are only semi-quantitative at points downstream of the blockage. They agree, qualitatively, with those found in experiments at ORNL[13] where maximum wake temperature rises were only about 200° F for blockages of 10%.

Clad and Fuel Temperatures

Temperatures of the clad and fuel at full reactor power, obtained by using the axial coolant temperature profile of Figure 9 (channels 1 - 4), are listed in Table 5. Calculational details may be found in Appendix A.

Of primary interest are the maximum clad and fuel temperatures, which occur at the point of maximum coolant temperature. Critical to these calculations are the clad-to-coolant heat transfer coefficient and the fuel thermal conductivity. (Correlations used are in Appendix A.) Calculations in Table 5 were made assuming that the clad-to-coolant heat transfer coefficient in the wake region was that given by a correlation that has been proven acceptable only in un-blocked coolant channels. Though it has been found that local coolant boiling may either not effect[14] or actually increase[5] the heat transfer coefficient, it is of some value to consider the effects of a decreased heat transfer coefficient on clad and fuel temperatures.

Table 6 shows the effects of varying the heat transfer coefficient

TABLE 5

COOLANT, CLAD AND FUEL TEMPERATURES

(Coolant Temperatures Average of Channels 1 - 4)

Axial Distance (inches)	Temperatures (^{o} F)				
	Coolant	Clad Surface (outer)	Clad Surface (inner)	Fuel Surface	Fuel Center
7.8	709	711	718	777	849
9.3	724	726	735	806	896
10.7	741	743	754	832	934
12.1	759	761	772	856	965
13.5	780	782	794	879	992
15.0	1800	1824	1882	2497	4148
16.0	1560	1582	1642	2248	3908
17.1	1480	1501	1561	2149	3767
18.5	1453	1456	1463	1538	1685
19.9	1393	1395	1402	1466	1587

TABLE 6

MAXIMUM CLAD AND FUEL TEMPERATURES AS A FUNCTION OF CLAD-TO-COOLANT HEAT TRANSFER COEFFICIENT AND FUEL THERMAL CONDUCTIVITY

(coolant temperature: 1800° F)

Heat Transfer Coefficient (Btu/(hr ft^2 ° F))	Temperatures (° F)				
	Clad Surface (outer)	Clad Surface (inner)	Fuel Surface	Fuel Center (normal fuel conductivity)	Fuel Center (10% decrease in conductivity)
20,904	1824	1882	2497	4148	4297
15,000	1834	1891	2506	4155	4304
10,000	1851	1908	2523	4169	4317
5,000	1902	1958	2573	4209	4354
1,000	2310	2362	2977	4496	4623
750	2480	2530	3145	4605	4732
350	clad melting		3258	4679	4806
300			3501	fuel melting	

in a range of 1% to 100% of the correlation predicted value of 20,904 Btu/(hr ft^2 ^{o} F). Note that clad melting occurs before any fuel melting, and that no fuel melting occurs unless the heat transfer coefficient approaches the extremely low value of 300 Btu/(hr ft^2 ^{o} F).

The effects of a decrease in fuel thermal conductivity by 10% is also shown in Table 6. Again, it is noted that clad melting precedes any fuel melting.

All fuel central temperatures listed were calculated assuming no fuel restructuring. Since restructuring does occur rather quickly, maximum fuel temperatures will be less than indicated, and, consequently, fuel melting is even more unlikely.

Mechanical Analysis

A rigorous analysis of thermal stresses would require a rather complex model which included both creep and two-dimensional temperature gradients. Such effort was deemed inappropriate for a conceptual design. Therefore, only an estimate of the maximum values of the thermal stresses was made by using the plane strain approximation. This method is normally acceptable when axial temperature gradients are small compared to radial gradients.[17] Neglecting thermal creep results in an overestimation of thermal stresses.

Table 7 lists the maximum hoop stresses predicted at various axial locations, using the coolant temperature profile of Figure 9, and compares them to the 0.2% offset yield strengths and the ultimate tensile strengths. Also listed are the predicted values of clad radii increase due to thermal expansion. Note that all stresses are below the 0.2% offset yield strengths.

TABLE 7

MAXIMUM CLAD THERMAL STRESSES VS. AXIAL LOCATION

Axial Distance (inches)	Clad Surface Temp. (^{o}F)	Hoop Stress (psi)	0.2% Offset Yield[16] Strength (psi)	Ultimate Tensile[15] Strength (psi)	Radial Clad Expansion (in)
7.8	711	931	23,000	68,000	.0007
9.3	726	1119	23,000	68,000	.0007
10.7	743	1232	23,000	68,000	.0008
12.1	761	1297	23,000	68,000	.0008
13.5	782	1324	23,000	68,000	.0008
15.0	1824	6235	10,000[a]	14,200[b]	.0025
16.00	1582	6825	15,000	22,900	.0020
17.1	1501	6860	15,000	27,000	.0019
18.5	1456	1417	15,500	30,500	.0018
19.9	1395	782	16,000	35,000	.0017

[a] extrapolated from 1500^{o} F

[b] estrapolated from 1700^{o} F

Table 8 presents the predicted clad stresses in the boiling region (0.75 in downstream of blockage) as a function of the clad-to-coolant heat transfer coefficient. Values of ultimate tensile strength are extrapolated above 1700° F and are, therefore, rather uncertain.

An estimate of the stresses due to the steep axial temperature gradient through the blockage is provided by:[18]

$$S = \tfrac{1}{2}E \left(\frac{dT}{dZ}\right) Za \qquad \text{Eq. 6}$$

where:

S = maximum value of clad stress due to axial temp. gradient

E = modulus of elasticity

$\frac{dT}{dZ}$ = axial temperature gradient

Z = clad thickness

a = thermal coefficient of expansion of the clad

Use of Eq. 6 results in the prediction of a stress of 1040 psi. This is the same order of magnitude as the stress of 6235 psi calculated for this region using the plane strain approximation. Consequently, as noted earlier, use of the plane strain approximation may be questionable.

All stress calculations were performed by assuming an effective clad thickness of 15 mils.[9] This value was obtained by subtracting the following losses from the design thickness of 20 mils:

fabrication tolerance: 1 mil

possible clad defects: 2 mils

erosion and corrosion: 1 mil

fuel-clad diffusion: 1 mil

The fabrication tolerance is the value used in the FTR conceptual pin design.[19] An inspection of the maximum diameter deviation of 36

TABLE 8

MAXIMUM CLAD THERMAL STRESSES IN WAKE REGION VS. CLAD-TO-COOLANT HEAT TRANSFER COEFFICIENT

Heat Transfer Coeff. (Btu/(hr ft^2 $^\circ$ F))	Clad Surface Temp. ($^\circ$ F)	Hoop Stress (psi)	Ultimate Tensile[15]a Strength (psi)	Radial Clad Expansion (in)
20,904	1824	6235	14,200	.0025
15,000	1834	6207	13,800	.0025
10,000	1851	6160	13,200	.0025
5,000	1902	6019	11,400	.0026
1,000	2310	4916	0	.0035

[a]estrapolated from 1700° F

pins prototypical to FTR fuel elements indicates this value may be conservative as the maximum deviation was 0.3 mils.[20]

The clad defect value is 10% of the design thickness as required by reference 9.

Extrapolation of corrosion rates listed in reference 9 (from 1450° F) and reference 16 (from 1750° F) results in a loss rate prediction of 4.5 mils per year at 1850° F. Thus, the assumed value of 1 mil is, again, probably conservative.

Similar extrapolations of effective clad loss due to fuel-clad reactions results in a loss rate of 0.78 mils per atm % burnup at 1850° F.[9]

Safety Analysis

The primary safety-related objective is the prevention of an accident that may damage reactor components. Generally, the likely source for such an incident is the molten fuel - coolant interaction. It is believed that the inherent safety features of this design makes the possibility of fuel melting and incident propagation extremely unlikely. These features include:

(1) Good Heat Transfer in the High Temperature Region: The average temperature in the boiling region is over 600° F below the saturation temperature and the adjacent bypass flow is about 1000° F subcooled. Thus, extreme voiding of the wake region is improbable,[2] and bubbles should collapse quickly, making dryout unlikely. This has been predicted theoretically and is being tested experimentally.[8]

(2) Clad Failure Unlikely: It has been shown that clad failure will not occur until the clad-to-coolant heat transfer coefficient reached a very low value of 5,000 Btu/(hr ft^2 ° F). Predictions of a critical

heat flux (CHF = 737,000 + 1.33 h_c $T_{subcool}$ [14]) indicate that the maximum design value (514,000 Btu/(hr ft^2 ^oF)) is quite acceptable.

(3) Clad Failure Before Fuel Melting: It was shown that clad melting would occur before the initiation of fuel melting. If clad melting occurred, it would likely happen in a rather small region, and the amount of fuel released into the coolant would not be enough to restrict coolant flow in the subassembly. Thus, in the event of clad failure, fuel particles released to the coolant are likely to be swept out of the wake to subassembly regions where they will be cooled by the normal coolant flow.

(4) Particle Collectors: Particle collectors will keep all debris within the subassembly, thus decreasing the chances of restricting coolant flow elsewhere in the reactor.

(5) No Incident Propagation: Large subcooling around the wake, the absence of large fission gas pressures in the fuel elements, and the barrier provided by the row of dummy pins between the wake and subassembly wall make the chances of an incident propagation within the wake or outside of the subassembly extremely unlikely. Further protection is provided by a subassembly can wall twice the thickness as those normally used in EBR-II.

Though the axial coolant temperature profiles were only semi-quantitative, the important calculations occurred at the location where the coolant temperature was the "known" saturation value. A saturation temperature of 1800^o F was assumed, though the actual value will be a few degrees less.

Consideration of superheat was neglected as it is virtually unknown in the EBR-II environment, and would likely be of importance only at the onset of boiling.

Neglect of fuel restructuring and thermal creep in the clad makes all calculations conservative. Furthermore, calculations were performed for the extreme case where boiling isn't initiated until full reactor power is obtained, although it is expected that boiling will occur somewhere between 52% and 89% of full power.

It is interesting to consider the effects on clad and fuel in the event of one of two extreme conditions. First, in the event of operation at 25% over normal full power, the maximum clad temperature is about 1900° F and the maximum fuel temperature is less than 4600° F. Neither clad failure nor fuel melting should occur. Secondly, consider operation at 25% over full power, a decrease by a factor of two of the clad-to-coolant heat transfer coefficient, and a 10% decrease in the fuel thermal conductivity. Maximum clad and fuel temperatures for this case are about 1935° F and 4762° F, respectively. Again clad failure does not occur, but fuel central temperatures are approaching the melting point (4800° F).

CONCLUSION

A conceptual design has been presented of a subassembly which is both safe and as prototypical of a commercial LMFBR subassembly as possible, given the limitations of EBR-II. Since no in-reactor boiling experiment with a subassembly containing a blockage has ever been performed (on a controlled basis), there is no direct experimental evidence to support the predicted behavior of the subassembly components. Consequently, many approximations and assumptions have been necessary, but it is felt that they were made in a manner which resulted in calculations being conservative.

Results from experiments to be conducted in Europe[8] and the creation of a subassembly thermal-hydraulic analysis code capable of handling reverse coolant flow would be extremely valuable for use in further evaluation of this design.

Finally, it is noted that the rather unprototypically low flow rates needed to assure that boiling occurs is primarily a consequence of the small cross-sectional areas of EBR-II subassemblies. A design suited to a reactor such as FTR would allow more prototypical flow rates.

REFERENCES

1. Artus, S.C., "A Gamma Heated Subassembly for Sodium Boiling Experiments," M.S. Thesis, University of Washington, Seattle, 1975.

2. Gregory, C.V., and Lord, D.J., "The Study of Local Blockages in Fast Reactor Sub-Assemblies," Journal of the British Nuclear Energy Society, 1974, Vol. 13:251-260.

3. Kirsch, D., "Investigations on the Flow and Temperature Distribution Down-Stream of Local Coolant Blockages in Rod Bundle Subassemblies," Nuclear Engineering and Design, 1974, Vol. 31:266-279.

4. Fontana, M.H. et al., "Temperature Distributions in a 19-Rod Simulated LMFBR Fuel Assembly With a Six-Channel Blockage," ORNL-TM-4448, May, 1974.

5. van Eerp, J.B., and Chawla, T.C., "Experimental Study of Coolant Crossflow and Subchannel Flow Behind a Blockage in a Simulated LMFBR Subassembly," Transactions of the American Nuclear Society, 1971, Vol. 14:746.

6. Hall. R.S., "Safety Instrumentation for the Sodium-Cooled Fast Reactor," Journal of the British Nuclear Energy Society, 1974, Vol. 13:173-181.

7. Judd, A.M., "Fuel Pin Failure Propagation in a Sodium Cooled Fast Reactor," Journal of the British Nuclear Energy Society, 1973, Vol. 12:35-42.

8. Smidt, D., and Schleisiek, K., "Fast Breeder Safety Against Local Failure Propagation," Transactions of the American Nuclear Society, 1975, Vol. 22:482-483.

9. Argonne National Laboratory, Guide for Irradiation Experiments in EBR-II, USAEC, 1975.

10. Rowe, D.S., "COBRA III-C: A Digital Computer Program for Steady State and Transient Thermal-Hydraulic Analysis of Rod Bundle Nuclear Fuel Elements," BNWL-1695, March, 1973.

11. Gosman, A.D. et al., Heat and Mass Transfer in Recirculating Flows, Academic Press, 1969.

12. Weisman, Joel, and Bowring, Robert W., "Methods for Detailed Thermal and Hydraulic Analysis of Water-Cooled Reactors," Nuclear Science and Engineering, 1975, Vol. 57:267.

13. Millhallen, M.K., and Sutey, A.M., "Subchannel Coolant Temperatures of EBR-II Instrumented Subassembly PNL-17 (XX02)," Transactions of the American Nuclear Society, 1970, Vol. 13:806-807.

14. Lurie, H., and Noyes, R.C., "Boiling Studies for Sodium Reactor Safety, Part II, Pool Boiling and Initial Forced Convection Tests and Analyses," NAA-SR-9477, 1964.

15. Metals Handbook, 1948 Edition, American Society for Metals, Cleveland, Ohio.

16. Conner, J.G., and Porembka, S.W., "Compendium of Properties and Characteristics for Selected LMFBR Cladding Materials," BMI-1900 UC-25-4, May, 1968.

17. Boley, B.A., and Weiner, J.H., Theory of Thermal Stresses, John Wiley and Sons, Inc., 1960.

18. McLain, S., and Martens, J.H., Reactor Handbook, Vol. IV, Engineering, Interscience Publishers, 1964, p. 275.

19. Stevens, E.G. et al., "FFTF Pin and Subassembly Conceptual Design Methods and Data," BNWL-1064 UC-80, June, 1970.

20. Myers, R.L., "Fabrication of Mark II Prototypic FFTF Fuel Subassembly for Sodium Flow Test," BNWL-1418 UC-25, June, 1970.

21. Glasstone, S., and Sesonske, A., Nuclear Reactor Engineering, Von Nostrand Reinhold Company, 1967.

22. Dwyer, O.E., "Heat Transfer to Liquid Metals Flowing In-Line Through Unbaffled Bundles: A Review," Heat Transfer in Rod Bundles, The American Society of Mechanical Engineers, December, 1968, p. 153.

23. Kerrisk, J.F., "PINTEMP: A Computer Program for Fuel Element Design Calculations," LA-5868-MS, February, 1975.

24. Yevick, J.F., ed., Fast Reactor Technology: Plant Design, MIT Press, 1966.

25. Bates, J.L., "High Temperature Thermal Conductivity of 'Round Robin' Uranium Dioxide," BNWL-1421 UC-25, July, 1970.

26. Golden, G.H., and Tokar, J.V., "Thermophysical Properties of Sodium," ANL-7323, 1967.

27. Jansing, W. et al., "Out of Pile Experiments with Prototype Fuel Elements for SNR-300," Fuel and Fuel Elements for Fast Reactors, Vol. 1.

APPENDIX A

Nomenclature

a	coefficient of thermal expansion of clad, $1/^{\circ}$ F
c_p	coolant heat capacity, Btu/(lb $^{\circ}$ F)
d	hydraulic diameter, ft
e	fraction fissile enrichment
E	modulus of elasticity for clad, psi
g	pin-to-pin clearance, ft
h_c	clad-coolant heat transfer coefficient, Btu/(hr ft^2 $^{\circ}$ F)
h_{gap}	fuel-clad heat transfer coefficient, Btu/(hr ft^2 $^{\circ}$ F)
k	thermal conductivity, Btu/(hr ft $^{\circ}$ F)
L_B	effective blockage radius, ft
L_R	flow reattachment length (wake length), ft
Nu	Nusselt number = $h_c d/k_{Na}$
p	coolant density, lb/ft^3
p'	porosity of fuel
Pe	Peclet number = $dvpc_p/k_{Na}$
q''	surface heat flux, Btu/(hr ft^2)
q'''	volumetric heat generation rate, Btu/(hr ft^3)
Q	total heat production within wake region, Btu/hr
r	radius, ft
Δr	increase in clad radius due to thermal expansion, ft
R_b	thermal resistance of blockage, (hr $^{\circ}$ F)/Btu
R_c	thermal resistance of coolant between wake and bypass flow, (hr $^{\circ}$ F)/Btu
R_t	resistance to turbulent heat transfer, (hr $^{\circ}$ F)/Btu
R_T	total thermal resistance between wake and bypass flow, (hr $^{\circ}$ F)/Btu
S	hoop stress at inner clad surface, psi

t	wake residence time, sec
v	coolant velocity, ft/hr
v'	Poisson's ratio for clad
V_w	coolant volume in wake, ft^3
w	blockage thickness, ft
x	effective mixing length, ft

subscripts

c	clad
f	fuel
fo	fuel center
fs	fuel surface
i	inner clad surface
Na	sodium
o	outer clad surface
25	U^{235}
28	U^{238}

Thermal Data and Analysis

Table 9 lists the volumetric heat generation rates at full reactor power for U^{235}, U^{238}, and iron. Axial locations are referenced to the bottom of the interlocking support grid.

Heat generation rates in U^{235} and U^{238} were calculated by using:

(1) relative fission rate distributions that would occur in a driver fuel subassembly in a nominal row 6 position of EBR-II (pp. 7-8, Appendix C, Ref. 9)

(2) the ratio of peak to axially-averaged fission rates in row 5 of EBR-II (p. 11, Appendix C, Ref. 9)

(3) fission rates at full reactor power in the center of a driver subassembly located in a INSAT position (p. 6, Appendix C, Ref. 9)

(4) a heavy atom density (100% theoretical) of 9.66 g/cm^3

(5) a heat rating of 196 Mev/fission (p. 12, Appendix C, Ref. 9)

Heat generation rates in iron were calculated by using gamma heating rates for a row 6 position of EBR-II (p. 23, Appendix C, Ref. 9) and an iron density of 8 g/cm^3.

The following assumptions were made:

(1) Flux shapes in an INSAT position (row 5) differ minimally from those in row 6. This is certainly true in the region of high enrichment for this design.

(2) The support grids have the same material consistency per unit length as a stainless steel dummy pin. The fraction of the total subassembly power added in this region is small enough to make the question of the validity of the approximation unimportant.

(3) Both radial power peaking and possible flux depressions resulting from different quantities and distributions of fissionable material,

TABLE 9

VOLUMETRIC HEAT GENERATION RATES IN U^{235}, U^{238}, AND IRON

Distance (in)	Heat Generation (Btu/(hr in^3)) U^{235}	U^{238}	Iron
0.00			$.208 \times 10^3$
0.45			.223
1.65			.278
2.55			.334
3.65			.446
4.80			.556
6.38			.779
7.50	1.381×10^5	4.6×10^3	1.39
8.18	1.330	5.6	1.81
8.85	1.355	6.6	2.01
9.53	1.388	7.2	2.21
10.20	1.421	7.8	2.26
10.88	1.454	8.1	2.30
11.55	1.486	8.4	2.34
12.23	1.506	8.6	2.38
12.90	1.527	8.8	2.42
13.58	1.532	8.8	2.46
14.25	1.537	8.9	2.51
14.93	1.529	8.8	2.46
15.60	1.520	8.7	2.42
16.28	1.495	8.5	2.38
16.95	1.470	8.3	2.33
17.63	1.437	8.0	2.29
18.30	1.404	7.7	2.25
18.98	1.370	7.1	2.13
19.65	1.335	6.4	1.96
20.33	1.331	5.4	1.78
21.00	1.352	4.4	1.45
21.73			1.11
23.70			.556
24.49			.446
25.86			.334
27.83			.223
28.50			.201

as compared to an EBR-II driver subassembly, are unimportant. Table 10 lists the relative fission rates that would occur for various radial positions in an EBR-II driver subassembly located in an INSAT position. It is evident that the total subassembly power may be well approximated by using subassembly centerline fission rates. Consideration of Table C-VIII of Ref. 9 leads to the observation that the expected U^{235} fission rate depression because of less fissionable material in the subassembly would be, at most, several percent.

TABLE 10

RELATIVE RADIAL FISSION RATES FOR EBR-II DRIVER SUBASSEMBLY IN INSAT[9]

	Relative Fission Rates		
Isotope	Nearest Core Center	Center of Subassembly	Furthest From Core Center
U^{235}	1.07	1.00	.93
U^{238}	.94	1.00	.89

The volumetric heat generation rate in the enriched UO_2 fuel is given by:

$$q_f''' = (q_{25}''' \, e + q_{28}''' \, (1-e)) \times (\% \text{ theoretical density}) \qquad \text{Eq. 7}$$

The heat flux at the outer surface of a fuel element is given by:

$$q'' = \frac{1}{2r_o} (q_f''' \, r_f^2 + q_c''' \, (r_o^2 - r_i^2)) \qquad \text{Eq. 8}$$

Table 11 lists the surface heat flux at full reactor power for fuel and dummy elements.

The outer clad surface temperature is given by:

$$T_o = \frac{q''}{h_c} + T_{Na} \qquad \text{Eq. 9}$$

TABLE 11

HEAT FLUXES FROM FUELED AND DUMMY ELEMENTS

(Full Reactor Power)

Distance (in)	— q'' (Btu(hr in^2)) — Fueled Element	Dummy Element
0.00	11.94	11.94
1.43	15.45	15.45
2.85	21.00	21.00
4.28	29.19	29.19
5.70	39.45	39.45
7.13	51.00	51.00
7.84	338.6	91.93
8.55	378.1	110.4
9.98	437.4	129.0
11.40	470.9	134.0
12.83	491.9	138.9
14.23	498.8	144.2
14.25	3570	144.3
15.68	3521	138.9
17.10	3393	133.5
18.25	3261	129.6
18.53	431.5	127.1
20.00	368.8	108.1
21.38	68.57	68.57
22.80	51.21	51.21
24.23	30.80	30.80
25.65	20.28	20.28
27.08	15.33	15.33
28.50	11.58	11.58

The following correlation was used for the clad-to-coolant heat transfer coefficient:[21]

$$Nu = 7 + .025\ Pe^{.8} \qquad \text{Eq. 10}$$

This correlation yields results that agree fairly well with experimental results for sodium flowing through unbaffled rod bundles of triangular pitch for Peclet numbers of the design range.[22]

The inner clad surface temperature is given by:

$$T_i = T_o + \frac{q'' r_o}{k_c} \ln \left(\frac{r_o}{r_i}\right) \qquad \text{Eq. 11}$$

Heat generation within the clad is neglected in this calculation.

The fuel surface temperature is given by:

$$T_{fs} = T_i + \frac{q''}{h_{gap}} \qquad \text{Eq. 12}$$

The gap coefficient is based upon beginning-of-life values recommended in Ref. 19 for FTR, which has the same diametrical gap and backfill gas as the design.

The fuel central temperature is obtained by solving the following for T_{fo}:

$$\int_{T_{fs}}^{T_{fo}} k\, dT \left(\frac{1 - p'}{1 + p'}\right) = \frac{q'' r_o}{2} \qquad \text{Eq. 13}$$

The term in parenthesis accounts for the fuel porosity.[23] It is assumed that no fuel restructuring occurs.

Mechanical Analysis

The radial expansion of the clad due to thermal stresses is given by:

$$\Delta r\Big|_{r_o} = a r_o T\Big|_{r_o} + \frac{a q'' r_o^2}{k_c} \left[\frac{1}{2} - \frac{r_i^2}{r_o^2 - r_i^2} \ln \left(\frac{r_o}{r_i}\right)\right] \qquad \text{Eq. 14}$$

This expression was obtained by multiplying Eq. 11 by r, integrating from r_i to r_o, and using the result in the relationship given in Ref. 17 (p. 291).

The maximum thermal stresses which occur in the clad are the tangential (hoop) and axial stresses at the inner surface. They are equal at this point and are given by:[17,24]

$$S = \frac{Ea}{2(1 - \nu')\ln(\frac{r_o}{r_i})} \left(T_{r_i} - T_{r_o}\right)\left[1 - \frac{2 r_o^2}{r_o^2 - r_i^2} \ln(\frac{r_o}{r_i})\right] \qquad \text{Eq. 15}$$

Thermal Conduction Between Wake and Bypass Flow

A simple model to take into account the effects of thermal conduction between the coolant and the wake region is presented here.

Consider the wake to be of cylindrical shape of length L_R (Fig. 7) and to contain the volume of liquid that would be contained in the 24 coolant channels extending the same distance downstream from the blockage. The temperature inside the wake is at its mean value, T_w, and the temperature of the bypass flow is at the mean value, T_b. There are three possible methods of heat transfer: conduction through the steel blockage, conduction through the coolant, and turbulent heat exchange.

The effective surface area for conduction through the coolant is the product of the pin-to-pin clearance, the wake length, and the 12 gaps separating the wake from the bypass flow, plus the flow areas of the 24 channels on the downstream end of the wake.

The effective surface area for conduction through the blockage is assumed to be the sum of the areas of the 24 blocked channels and the cross-sectional area of the cladding within the blockage.

If it is assumed that there is no temperature drop between the upstream side of the blockage and the coolant there, then the mean temperature difference between the bypass flow and the wake is:

$$\Delta T = QR_T \qquad \text{Eq. 16}$$

where Q is the total heat produced within the wake and R_T is the total thermal resistance between the wake and bypass flow. R_T is given by:

$$R_T^{-1} = \frac{1}{R_b} + \frac{1}{R_c} + \frac{1}{R_t} \qquad \text{Eq. 17}$$

where the thermal resistance of the blockage is:

$$R_b = \frac{w}{(24A_c + 12\ (r_o^2 - r_i^2))\ k_b} = .505\ \frac{hr\ ^oF}{Btu} \qquad \text{Eq. 18}$$

The thermal resistance through the coolant is given by:

$$R_c = \frac{x}{(24A_c + 12L_Rg)\ k_{Na}} = .106\ \frac{hr\ ^oF}{Btu} \qquad \text{Eq. 19}$$

The effective mixing length for thermal conduction in the coolant, x, has been approximated by the distance between area centroids of the blockage and bypass flow (.0310 ft), using the one-sixth geometry of Fig. 8. The recirculation length, L_R, has been estimated at 3.5 L_B, where L_B is the effective radius of the blockage (0.5 in). The latter value has been used in accordance with experimental evidence and theoretical predictions of reattachment lengths of three to three and one-half times blockage radii.[2,3]

The resistance to turbulent heat transfer, by inspection of Eq. 1, is:

$$R_t = \frac{t}{\rho c_p V_w} \qquad \text{Eq. 20}$$

The total thermal resistance then is:

$$R_T = 11.4 + \frac{14.5}{t}\quad \frac{hr\ ^oF}{Btu} \quad (t \text{ in seconds}) \qquad \text{Eq. 17}$$

For a flow rate of 0.5×10^6 lb/(hr ft^2) (t = .34 sec), Eq. 18 indicates that about 20% of the heat added in the wake is lost through conduction. For Re_{BL} of about 10^6 (t = .009 sec), less than 1% of the heat is transported through molecular conduction in agreement with the predictions of Kirsch (see p. 20).

The total heat produced within the wake is:

$$Q = q''_{wake}\, 12\pi (2r_o)\, L_R = .1054\, q''_{wake} \qquad \text{Eq. 21}$$

Substituting Eq. 17 and Eq. 21 into Eq. 16 results in Eq. 5:

$$T = \frac{.1054\, q''_{wake}}{11.4 + \frac{14.5}{t}} \times (\text{fraction operating power}) \qquad \text{Eq. 5}$$

The maximum wake temperature is then given by:

$$T_{max} = 700 + 1.6\Delta T + (800 - 700) \times (\text{fract. operating power}) \qquad \text{Eq. 22}$$

since the inlet temperature is 700° F and the average temperature of the bypass flow at full reactor power is about 800° F.

Correlations for Materials Properties

Correlations for materials properties used in the thermal and mechanical analysis are listed here. Where noted with an asterik, curve fitting to data in the given reference was made to obtain the correlation.

(1) Liquid Sodium

thermal conductivity(23)

$$k_{Na} = 53.05 - .0172T + 1.56 \times 10^{-6} T^2$$

(2) Stainless Steel - 316

thermal conductivity(23)

$$k_c = 7.991 + 5.033 \times 10^{-3} T - 2.579 \times 10^{-7} T^2$$

coefficient of thermal expansion*(15)

$a = 6.92 \times 10^{-6} + 2.789 \times 10^{-9} T$

Poisson's ratio (stainless steel)[23]

$v' = 0.3$

modulus of elasticity*[16]

$E = 2.956 \times 10^{7} - 7100T$

(3) Helium

fuel-clad gap heat transfer coefficient at beginning-of-life[19]

$h_{gap} = 830$ Btu/(hr ^{o} F ft^{2})

(4) UO_2

thermal conductivity integral[25]

$$\int_0^T k\, dT = 5.228T - 1.767 \times 10^{-3} T^2 + 3.795 \times 10^{-7} T^3 - 4.240 \times 10^{-11} T^4 + 2.414 \times 10^{-5} T^5$$

APPENDIX B

COBRA III-C Input Data and Correlations

A fine description of COBRA III-C is contained in Ref. 10; therefore, only a listing of the important input data and correlations used is made.

(1) Fluid Properties: Ref. 26

(2) Flow Correlations

friction factor:[21,27] $f = .316\ Re^{-.250}$

subcooled voiding: none

friction multiplier: homogeneous model

wall viscosity: correction to friction factor included

(3) Axial Heat Flux

z/L	Relative Flux	z/L	Relative Flux
.000	.018	.500	5.419
.050	.023	.550	5.345
.100	.032	.600	5.151
.150	.044	.640	4.950
.200	.056	.650	.655
.250	.077	.700	.560
.275	.514	.750	.104
.300	.574	.800	.078
.350	.665	.850	.047
.400	.715	.900	.031
.450	.747	.950	.023
.499	.757	1.000	.018

(4) Subchannel Layout and Dimensions (1/6 geometry - see Fig. 8)

Subchannel No.	Area (in^2)	Wetted Perimeter (in)	Heated Perimeter (in)
1 - 9	.0120	.3613	.3613
10, 12	.0268	.7883	.4215
11	.0230	.6363	.3613

centroid distances:

Typical Adjacent Channels	Centroid Distance (in)
2 - 3	0.159
5 - 10	0.187
10 - 11	0.138

(5) Rod Layout, Dimensions and Power Factors (see Fig. 8)

Rod	Diameter (in)	Relative Rod Power
1 - 6	.230	1.75
7 - 10	.230	.2083

(6) Calculational Variables

crossflow resistance factor: 0.5 (The actual value used is insignificant.[10])

momentum turbulent factor: 0

parameter, s/L:[10] 0.5

channel length: 28.5 in

flow convergence factor: 1.0×10^{-3}

(7) Turbulent Mixing Correlations

subcooled mixing: $0.0120(D/s)\ Re^{-0.1}$ (This value was used successfully in predicting temperatures in an instrumented subassembly operated in EBR-II[13])

two-phase mixing: same as subcooled mixing

thermal conduction geometry factor: 1

(8) Operating Conditions

inlet temperature: 700.0° F

mass velocity: 0.5×10^{6} Btu/(hr ft^2) x (full power)

average heat flux: 0.0542×10^{6} Btu/(hr ft^2) x (full power)

flow split to give equal pressure gradients at subchannel inlets

APPENDIX E

Procedures and Instrumentation for EBR-II Sodium Boiling Experiments

R. Crowe